Chemistry Research Journal, 2022, 7(3):1-18

Available online www.chemrj.org

Research Article

ISSN: 2455-8990
CODEN(USA): CRJHA5

A theoretical study of the relationships between electronic structure of 2-aryladenine derivatives and percentage of inhibition of radioligand binding in human A_{2A} and A_{2B} adenosine receptors

Juan S. Gómez-Jeria*[1,2], Alonso Ibertti-Arancibia[1], Lilian Olarte-Lezcano[1]

[1]Quantum Pharmacology Unit, Department of Chemistry, Faculty of Sciences, University of Chile. Las Palmeras 3425, Santiago 7800003, Chile.
[2]Glowing Neurons Group, CP 8270745 Santiago, Chile.
Corresponding author: facien03@uchile.cl

Abstract Employing the Klopman-Peradejordi-Gómez formal method we have analyzed the relationships between the electronic structure and the percentage of inhibition of radioligand binding for the case of a group of 2-aryladenine derivatives interacting with the human A_{2A} and A_{2B} adenosine receptors. The ultimate goal is suggesting modifications of the structure of 2-aryladenine derivatives to enhance the percentage of inhibition of radioligand binding. All electronic structure calculations were carried out with the Gaussian set of programs and with software written in this Unit. For each case, we found statistically significant relationships. The equations relate the variation of the percentage of inhibition to the variation of the numerical values of a set of local atomic reactivity indices. These indices allowed us to propose possible atom-site non-bonded interactions that could serve as a basis for the development of new molecules with enhanced or diminished activities.

Keywords Adenosine receptors, QSAR, Klopman-Peradejordi-Gómez method, receptor affinity, 2-aryladenine derivatives, local atomic reactivity indices, chemical reactivity

Introduction

Adenosine receptors (ARs) comprise a group of G protein-coupled receptors, which intervene in the physiological actions of adenosine. This group comprises four members, named A_1, A_{2A}, A_{2B}, and A_3 receptors, which are extensively distributed in nearly all human body tissues and organs [1, 2]. The action of caffeine and theophylline on these receptors produces the stimulating effects of coffee, chocolate and tea [3].

Adenosine tone and ARs are involved in the modulation of synaptic activity and excitotoxicity, the control of neurotrophin levels and functions and the regulation of protein degradation mechanisms. ARs play also a range of roles in neuroinflammation, Parkinson's, Alzheimer's and Huntington's diseases, epileptic seizures and in brain ischemia as well as the control of cognition and pain. Numerous studies indicate that adenosine signal transduction is involved in asthma and chronic obstructive pulmonary diseases as well as in renal failure. Adenosine has a critical role in preserving cartilage and chondrocyte homeostasis under physiological conditions and in a selective protection against the beginning of osteoarthritis. ARs agonists and/or antagonists may also possibly be employed in the fight against diabetes mellitus and obesity because they act to normalize lipolysis, insulin sensitivity and thermogenesis. A_{2A} antagonists may enhance tumor immunotherapy in cancer treatment protocols. This is not an

exhaustive list [4-14]. The importance of these receptors led to the synthesis and testing of many molecular systems with the aim of finding compounds modulating the action of the ARs [15-30].

In our Unit, we have carried out studies of the relationships between electronic structure and ARs receptor affinities of two different groups of molecules [31, 32]. In this paper, we report the results of the application of the same methodology to a group of 2-aryladenine derivatives. We expect that the progressive accumulation of formal QSAR results will help to provide a better understanding of the molecule-ARs interactions.

Methods, Models and Calculations [33]

The Method

To carry out this study we employed the Klopman-Peradejordi-Gómez (KPG) method [34, 35]. This formal method relates activity with electronic structure through a linear relationship. The primitive form of this relationship was originally developed and employed by Peradejordi et al. [36] The actual version includes twenty local atomic reactivity indices per atom. The for any biological activity (BA) we have [37-44]:

$$\log(BA)=a+b\log\left(M_D\right)+\sum_{o=1}^{subs}\rho_o+\sum_{i=1}^{Z}\left[e_iQ_i+f_iS_i^E+s_iS_i^N\right]+$$
$$+\sum_{i=1}^{Z}\sum_{m=(HOMO-2)^*,i}^{(HOMO)^*,i}\left[h_i\left(m\right)F_i(m^*)+j_i\left(m\right)S_i^E\left(m^*\right)\right]+$$
$$+\sum_{i=1}^{Z}\sum_{m'=(LUMO)^*,i}^{(LUMO+2)^*,i}\left[r_i\left(m'\right)F_i(m'^*)+t_i\left(m'\right)S_i^N\left(m'^*\right)\right]+$$
$$+\sum_{i=1}^{Z}\left[g_i\mu_i^*+k_i\eta_i^*+o_i\omega_i^*+z_i\zeta_i^*+w_jQ_i^{*,max}\right] \quad (1)$$

where a, b, e_i, f_i, s_i $h_i(m)$, $j_i(m)$, $r_i(m')$, $t_i(m')$, g_i, k_i, o_i, z_i and w_i are constants to be determined, M_D is the mass of the drug and ρ_o is the orientational effect of the o-th substituent. Q_j is the net charge of the atom j, S_j^E and S_j^N are, respectively, the total atomic electrophilic and nucleophilic superdelocalizabilities of atom j. $F_j(m)$ and $F_j(m')$ are, respectively, the electron populations (Fukui index) of the occupied (m) and vacant (m′) local molecular orbitals (OMs) localized on atom j. $S_j^E(m)$ is the electrophilic superdelocalizability of the local OM m localized on atom j. The last terms, derived by one of the authors (J.S. G.-J.), are: μ_j the local atomic electronic chemical potential of atom j, η_j the local atomic hardness of the atom j, ω_j the local atomic electrophilicity of atom j, ς_j the local atomic softness of the atom j and Q_j^{max} (the maximum amount of electronic charge that atom j can accept) [44]. They are not the same local indices derived in Density Functional Theory because they have the same units that the global equivalents (in fact the new ones were derived within the Hartree-Fock scheme [44]). The MOs having an asterisk (*) correspond to the so-called Local Molecular Orbitals (LMO) of each atom. For atom p, the LMOs are the subset of the molecule's MOs having an electron population greater than 0.01e on p. In this study, we have considered the three highest occupied local MOs and the three lowest empty local MO of each atom. This restriction is not mandatory and more local MOs may be included if necessary.

Then, for a system of n molecules, we have n equations. The first condition that this linear system of equations 1 must satisfy to be solved is that each equation must have the same number of terms. This condition is satisfied only by selecting and using a group of atoms common to all the molecules. This group is called the common skeleton. The number of atoms of this common skeleton defines the index Z of Eq. 1. The second condition is that we must have at least the same number of equations than the total number of indices of the common skeleton and the other terms of Eq. 1. For example, if we have 20 atoms represented by 400 local atomic reactivity indices, we need at least

400 equations! Because of this reason, we used the linear multiple regression analysis (LMRA) to detect those indices associated with the variation of the values of the biological activity analyzed. This method has produced excellent results for various biological activities and receptors [31, 45-55].

Selection of Molecules and Biological Activities

The molecules were taken from a recent study [25]. The data selected for our study is the percentage of inhibition of radioligand binding at a concentration of 10 μM of the tested compounds [25]. Their general formula and receptor affinities are displayed, respectively, in Fig. 1 and Table 1.

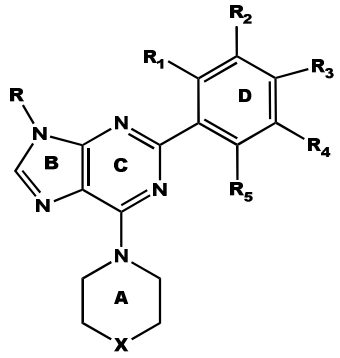

Figure 1: General formula of 2-aryladenine derivatives

Table 1: 2-aryladenine derivatives and percentage of inhibition of radioligand binding

Mol.	**R**	**X**	**R_1**	**R_2**	**R_3**	**R_4**	**R_5**	**log(A_{2A}) HeLa-A_{2A} cells**	**log(A_{2B}) HEK-293-A_{2B} cells**
1	Me	NMe	OH	H	H	H	H	1.77	1.56
2	Me	NMe	H	OH	H	H	H	0.62	1.68
3	Me	NMe	H	Cl	H	H	H	1.32	1.28
4	Me	NMe	H	Cl	Cl	H	H	1.4	1.45
5	Me	CH_2	OH	H	H	H	H	1.87	1.48
6	Me	CH_2	OH	OH	H	H	H	1.38	1.41
7	Me	CH_2	Cl	H	H	H	H	1.56	1.51
8	Me	CH_2	Cl	H	H	Cl	H	0.38	1.49
9	Me	CH_2	H	OH	H	H	H	1.74	1.47
10	Me	CH_2	H	Cl	H	H	H	1.23	1.38
11	H	NMe	Cl	H	H	Cl	H	0.96	1.11
12	H	NMe	H	OH	H	H	H	0	1.43
13	H	NMe	H	Cl	H	H	H	1.72	1.48
14	H	NMe	H	Cl	Cl	H	H	1.08	1.38
15	H	NMe	H	CF_3	Cl	H	H	1.5	1.4
16	H	NMe	H	H	OH	H	H	1.57	1.72
17	H	NMe	H	H	Cl	H	H	1.2	0.79
18	H	CH_2	Cl	H	H	Cl	H	1.32	1.08
19	H	CH_2	H	Cl	H	H	H	1.64	--
20	H	CH_2	H	Cl	Cl	H	H	0.84	-0.15
21	H	CH_2	H	H	Cl	H	H	--	0.15

Calculations

The electronic structure of all molecules was calculated within the Density Functional Theory (DFT) at the B3LYP/6-31g(d,p) level after full geometry optimization. The Gaussian 16 suite of programs was used [56]. All the data to calculate the numerical values of the local atomic reactivity indices was obtained from the Gaussian results with the D-Cent-QSAR software [57]. All electron populations smaller than or equal to 0.01e were considered as being zero. Negative electron populations coming from Mulliken Population Analysis were corrected [58]. We made use of Linear Multiple Regression Analysis (LMRA) techniques to find a statistically significant equation. The Statistica software was used [59]. The common skeleton for this case is shown in Fig. 2.

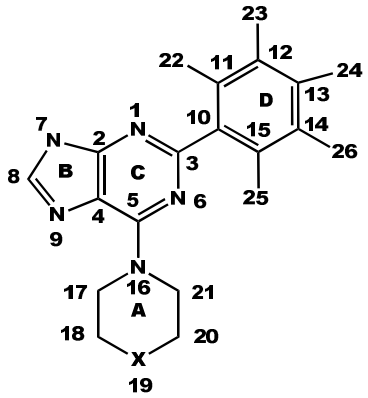

Figure 2: Common skeleton

Results

Results for the percentage of inhibition of radioligand binding of test compounds at human A_{2A} receptors.

The best equation obtained was:

$$\log(A_{2A}) = 14.31 - 1.69F_{26}(HOMO)^* - 0.45S_{12}^{E}(HOMO)^* - 2.02\mu_{20}^{*} + 2.81F_{25}(HOMO)^* - 7.75F_{20}(LUMO+1) + 2.43F_{25}(HOMO-2)^* - 0.001S_{15}^{N}(LUMO+2)^* \quad (2)$$

with n=20, R=0.97, R^2=0.94, adj-R^2=0.90, F(7,12)=25.421 (p<0.00000) and SD=0.16. No outliers were detected and no residuals fall outside the ±2σ limits. Here, F_{26}(HOMO)* is the electron population of the highest occupied local molecular orbital of atom 26, S_{12}^{E}(HOMO)* is the electrophilic superdelocalizability (ESD) of the highest occupied local molecular orbital of atom 12, μ_{20}^{*} is the local atomic electronic chemical potential of atom 20, F_{25}(HOMO)* is the electron population of the highest occupied local molecular orbital of atom 25, F_{20}(LUMO+1)* is the electron population of the second lowest empty local molecular orbital of atom 20, F_{25}(HOMO-2)* is the electron population of the third highest occupied local molecular orbital of atom 25 and S_{15}^{N}(LUMO+2)* is the nucleophilic superdelocalizability (NSD) of the third lowest empty local molecular orbital of atom 15. Tables 2 and 3 show, respectively, the beta coefficients, the results of the t-test for significance of coefficients and the matrix of squared correlation coefficients for the variables of Eq. 2. There are no significant internal correlations between independent variables (Table 3). Figure 3 displays the plot of observed *vs.* calculated values.

Table 2: Beta coefficients and t-test for significance of coefficients in Eq. 2

	Beta	t(12)	p-level
F_{26}(HOMO)*	-0.29	-3.56	0.004
S_{12}^{E}(HOMO)*	-0.53	-6.28	0.00004
μ_{20}^{*}	-0.48	-5.41	0.0002
F_{25}(HOMO)*	0.46	5.87	0.00008
F_{20}(LUMO+1)*	-0.50	-4.92	0.0004
F_{25}(HOMO-2)*	0.28	2.95	0.01
S_{15}^{N}(LUMO+2)*	-0.21	-2.55	0.025

Table 3: Matrix of squared correlation coefficients for the variables in Eq. 2

	F_{26}(HOMO)*	S_{12}^{E}(HOMO)*	μ_{20}^{*}	F_{25}(HOMO)*	F_{20}(LUMO+1)*	F_{25}(HOMO-2)*
S_{12}^{E}(HOMO)*	0.01	1.00				
μ_{20}^{*}	0.12	0.09	1.00			
F_{25}(HOMO)*	0.00	0.02	0.02	1.00		
F_{20}(LUMO+1)*	0.05	0.05	0.07	0.03	1.00	
F_{25}(HOMO-2)*	0.04	0.07	0.01	0.01	0.33	1.00
S_{15}^{N}(LUMO+2)*	0.07	0.01	0.07	0.05	0.14	0.00

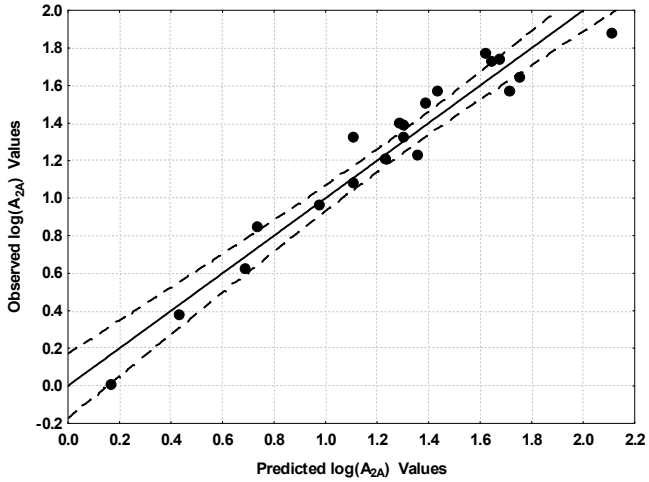

Figure 3: Plot of predicted vs. observed log(A_{2A}) values (Eq. 2). Dashed lines denote the 95% confidence interval

The associated statistical parameters of Eq. 2 indicate that this equation is statistically significant and that the variation of the numerical values of a group of seven local atomic reactivity indices of atoms constituting the common skeleton explains about 90% of the variation of log(A_{2A}). Figure 3, spanning about 1.9 orders of magnitude, shows that there is a good correlation of observed *versus* calculated values.

Results for the percentage of inhibition of radioligand binding of test compounds at human A_{2B} receptors.

The best equation obtained was:

$$\log\left(A_{2B}\right)=8.58-1.34F_{9}(\text{HOMO-2})^{*}-0.60F_{24}(\text{LUMO+1})^{*}-0.21S_{14}^{E}(\text{HOMO-1})-0.84\eta_{18}^{*} \quad (3)$$

with n=20, R=0.95, R^2=0.91, adj-R^2=0.88, F(4,15)=37.474 (p<0.00000) and SD=0.16. No outliers were detected and no residuals fall outside the ±2σ limits. Here, F_9(HOMO-2)* is the electron population of the third highest occupied local molecular orbital of atom 9, F_{24}(LUMO+1)* is the electron population of the second lowest empty local molecular orbital of atom 24, S_{14}^{E}(HOMO-1)* is the electrophilic superdelocalizability of the second highest occupied local molecular orbital of atom 14 and η_{18}^{*} is the local atomic hardness of atom 18. Tables 4 and 5 show the beta coefficients, the results of the t-test for significance of coefficients and the matrix of squared correlation coefficients for the variables of Eq. 3. There are no significant internal correlations between independent variables (Table 5). Figure 5 displays the plot of observed *vs.* calculated values.

Table 4: Beta coefficients and t-test for significance of coefficients in Eq. 3

	Beta	t(15)	p-level
F_9(HOMO-2)*	-0.61	-6.47	0.00001
F_{24}(LUMO+1)*	-0.35	-3.77	0.002
S_{14}^{E}(HOMO-1)*	-0.29	-3.47	0.003
η_{18}^{*}	-0.25	-3.12	0.007

Table 5: Matrix of squared correlation coefficients for the variables in Eq. 3

	F_9(HOMO-2)*	F_{24}(LUMO+1)*	S_{14}^E(HOMO-1)*	η_{18}^*
F_9(HOMO-2)*	1.00			
F_{24}(LUMO+1)*	0.24	1.00		
S_{14}^E(HOMO-1)*	0.03	0.01	1.00	
η_{18}^*	0.01	0.00	0.02	1.00

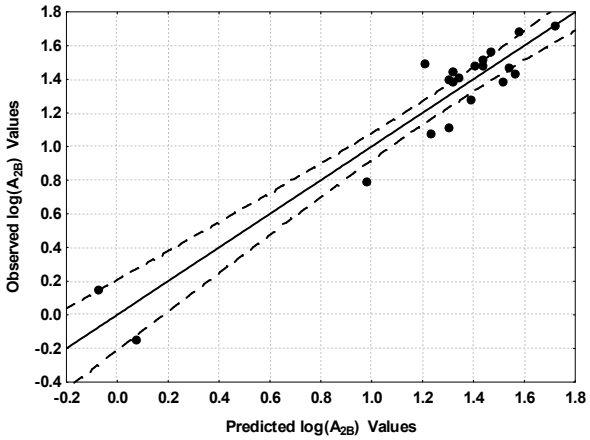

Figure 5: Plot of predicted vs. observed log(A_{2B}) values (Eq. 3). Dashed lines denote the 95% confidence interval

The associated statistical parameters of Eq. 3 indicate that this equation is statistically significant and that the variation of the numerical values of a group of four local atomic reactivity indices of atoms constituting the common skeleton explains about 88% of the variation of log(A_{2B}). Figure 5, spanning about 1.8 orders of magnitude, shows that there is a good correlation of observed *versus* calculated values.

Local Molecular Orbitals

Tables 6 and 7 show the local molecular orbitals of atoms appearing in Eqn. 2 and 3.

Table 6: Local Molecular Orbitals of atoms 8, 9, 12, 14 and 15.

Mol.	Atom 8	Atom 9	Atom 12	Atom 14	Atom 15
1 (86)	84π85π86π- 87π88π89π	84π85π86π- 87π88π89π	83π84π85π- 87π88σ89π	82π84π85π- 87π89π90π	82π83π84π- 87π88σ89π
2(86)	84π85π86π- 87π88π89π	84π85π86π- 87π88π89π	83π84π85π- 87π88π89π	83π84π85π- 87π89π90π	83π84π85π- 87π88π89π
3(90)	87σ89π90π- 91π92π93π	87σ89π90π- 92π93π94π	86π88π89π- 91π92π93π	87σ88π89π- 91π92π93π	87σ88π89π- 91π92π93π
4(98)	95σ97π98π- 99π100π101π	95σ97π98π- 100π101π103π	94π96π97π- 99π100π101π	93π94π97π- 99π100π101π	95σ96π97π- 99π100π101π
5(82)	79σ80σ82π- 83π84π85π	79σ80σ82π- 83π84π85π	79π80π81π- 83π84π85π	80π81π82π- 83π85π86π	80π81π82π- 83π84π85π
6(86)	82π83σ85π- 87π88π89π	82π83σ85π- 87π88π89π	84π85π86π- 87π88π90π	84π85π86π- 89π90π91π	84π85π86π- 87π88π90π
7(86)	84σ85σ86π- 87π88π89π	84σ85σ86π- 87π88π89π	83π84π85π- 87π88π89π	83π84π85π- 87π88π89π	83π84π86π- 87π88π89π
8(94)	91π92σ94π- 95π97π98π	91π92σ94π- 97π99π100π	91π92π93π- 95π96π98σ	91π92π93π- 95π96π97π	92π93π94π- 95π96π98σ

9(82)	79σ80π82π- 83π84π85π	78π79σ82π- 83π84π85π	71σ80π81π- 83π84π85π	78π80π81π- 83π85π86π	80π81π82π- 83π84π85π
10(86)	84σ85π86π- 87π88π 89π	82π84σ86π - 88π89π90π	80π83π85π- 87π88π89π	82π83π85π- 87π88π89π	84σ85π86π- 87π88π89π
11(94)	91π 93π94π- 95π96π97π	91π93π94π- 95π96π97π	90π91π92π- 95π96π98σ	90π92π93π- 95π96π97π	91π92π93π- 95π96π98σ
12(82)	80π81π82π- 83π84π85π	80π81π82π- 83π84π85π	79π80π81π- 83π84π85π	79π80π81π- 83π85π86π	78σ80π81π- 83π84π85π
13(86)	83σ85π86π- 87π88π89π	83σ85π86π- 87π88π89π	83σ84π85π- 87π88π89π	83σ84π85π- 87π88π89π	83σ84π85π- 87π88π89π
14(94)	91σ93π94π- 95π96π97π	91σ93π94π- 96π97π99π	90π92π93π- 95π96π97π	89π90π93π- 95π96π97π	91σ92π93π- 95π96π97π
15(102)	99σ101π102π- 103π104π105π	99σ101π102π- 104π105π106π	98π100π101π- 103π104π105π	98π100π101π- 103π104π105π	99σ100π101π- 103π104π105π
16(82)	80π81π82π- 83π84π85π	80π81π82π- 83π84π85π	78π80π81π- 84π85π86π	80π81π82π- 83π84π85π	80π81π82π- 83π84π85π
17(86)	83σ85π86π- 87π88π89π	84π85π86π- 87π88π89π	82π84π85π- 87π88π89π	82π84π85π- 87π88π89π	83σ84π85π- 87π88π89π
18(90)	87σ88σ90π- 91π93π94π	87σ88σ90π- 93π95π96π	87π88π89π- 91π92π94σ	84π87π89π- 91π92π93π	88π89π90π- 91π92π94σ
19(82)	80π81π82π- 83π84π85π	78π79σ82π- 83π84π85π	78π80π81π- 83π84π85π	78π80π81π- 83π84π85π	80π81π82π- 83π84π85π
20(90)	88σ89π90π- 91π92π93π	85σ88σ90π- 92π93π95π	86π87π89π- 91π92π93π	87π89π90π- 91π92π93π	88σ89π90π- 91π92π93π
21(82)	80σ81π82π- 83π84π85π	77σ80σ82π- 83π84π85π	78π79π81π- 83π84π85π	79π81π82π- 83π84π85π	80σ81π82π- 83π84π85π

Table 7: Local Molecular Orbitals of atoms 18, 20, 24, 25 and 26

Mol.	Atom 18	Atom 20	Atom 24	Atom 25	Atom 26
1 (86)	76σ85σ86σ- 98σ99σ100σ	76σ85σ86σ- 97σ98σ99σ	68σ71σ75σ- 94σ98σ99σ	73σ74σ75σ- 94σ98σ99σ	72σ73σ76σ- 92σ94σ101σ
2(86)	75σ84σ86σ- 96σ97σ98σ	78σ84σ86σ- 97σ98σ99σ	69σ74σ76σ- 95σ95σ98σ	72σ73σ74σ- 92σ93σ95σ	64σ73σ76σ- 95σ96σ98σ
3(90)	81σ89σ90σ- 100σ102σ103σ	81σ89σ90σ- 100σ102σ103σ	74σ75σ76σ- 95σ99100σ	74σ77σ78σ- 97σ98σ99σ	77σ78σ82σ- 95σ99σ100σ
4(98)	89σ97σ98σ- 109σ111σ112σ	89σ97σ98σ- 109σ111σ112σ	94π 96π 97π- 99π102σ103π	73σ80σ8σ1- 102σ105σ106σ	80σ81σ88σ- 102σ105σ108σ
5(82)	75σ76σ82σ- 92σ96σ97σ	79σ81σ82σ- 92σ95σ97σ	67σ69σ70σ- 89σ90σ94σ	61σ67σ70σ- 89σ90σ94σ	65σ67σ69σ- 88σ89σ90σ
6(86)	81σ84σ85σ- 95σ97σ101σ	81σ84σ85σ- 94σ95σ98σ	75σ77σ79σ- 94σ95σ97σ	74σ76σ79σ- 93σ94σ96σ	72σ74σ77σ- 93σ94σ96σ
7(86)	80σ85σ86σ- 95σ96σ100σ	80σ83σ86σ- 95σ100σ101σ	68σ69σ70σ- 91σ92σ95σ	70σ71σ73σ- 91σ93σ95σ	70σ71σ73σ- 91σ95σ96σ
8(94)	88σ90σ94σ- 104σ109σ110σ	88σ91σ94σ- 104σ110σ112σ	71σ74σ76σ- 98σ99σ106σ	76σ77σ80σ- 98σ99σ106σ	88π91π93π- 96π98σ99σ
9(82)	77σ80σ82σ- 91σ92σ93σ	77σ80σ82σ- 91σ96σ99σ	69σ70σ71σ- 89σ91σ92σ	66σ67σ69σ- 88σ89σ90σ	69σ70σ71σ- 89σ91σ92σ

10(86)	78σ81σ86σ-95σ96σ101σ	83σ85σ86σ-95σ101σ103σ	70σ71σ72σ-91σ95σ96σ	65σ70σ73σ-93σ94σ95σ	71σ73σ79σ-91σ95σ96σ
11(94)	87σ93σ94σ-105σ106σ107σ	83σ93σ94σ-105σ106σ107σ	72σ75σ76σ-98σ99σ107σ	74π76σ77σ-98σ99σ105σ	90π92π93π-96π98σ99σ
12(82)	75σ80σ82σ-92σ93σ94σ	75σ80σ82σ-93σ94σ95σ	65σ70σ72σ-91σ92σ93σ	69σ70σ71σ-89σ90σ91σ	69σ71σ72σ-91σ92σ93σ
13(86)	79σ85σ86σ-96σ97σ98σ	79σ85σ86σ-96σ97σ98σ	70σ71σ72σ-91σ95σ96σ	73σ74σ75σ-94σ95σ96σ	74σ75σ78σ-91σ95σ96σ
14(94)	87σ93σ94σ-105σ107σ108σ	87σ93σ94σ-105σ107σ108σ	90π92σπ93π-95π98σ99π	69σ76σ77σ-98σ101σ103σ	70σ76σ77σ-98σ101σ104σ
15(102)	95σ101σ102σ-112σ113σ114σ	95σ101σ102σ-112σ113σ114σ	98π100π101π-103π106π107σ	88σ89σ94σ-107σ110σ111σ	86σ87σ88σ-107σ111σ112σ
16(82)	80σ81σ82σ-92σ93σ94σ	80σ81σ82σ-93σ94σ95σ	80π 81π 82π-83π86π87π	60σ67σ72σ-90σ91σ92σ	60σ67σ72σ-88σ91σ92σ
17(86)	79σ85σ86σ-96σ98σ99σ	79σ85σ86σ-96σ97σ98	81π 84π 85π-87π91σ92π	74σ75σ78σ-91σ94σ95σ	73σ74σ75σ-91σ95σ96σ
18(90)	85σ87σ90σ-100σ101σ105σ	84σ85σ90σ-100σ104σ106σ	67σ71σ72σ-94σ95102σ	71σ72σ73σ-94σ95σ99σ	84π87π89π-92π94σ95σ
19(82)	76σ77σ82σ-91σ92σ95σ	80σ81σ82σ-91σ95σ96σ	65σ67σ67σ-87σ91σ92σ	61σ66σ69σ-90σ91σ92σ	67σ69σ75σ-87σ90σ91σ
20(90)	85σ89σ90σ-100σ101σ105σ	85σ89σ90σ-100106107	87π 89π 90π-91π94σ95π	86σ87σ89σ-92σ94σ97σ	72σ73σ81σ-94σ97σ100σ
21(82)	77σ81σ82σ-91σ92σ95σ	77σ81σ82σ-91σ95σ98σ	78π 81π 82π-83π87σ88π	66σ69σ75σ-87σ90σ91σ	66σ67σ69σ-87σ91σ92σ

Discussion

Molecular Electrostatic Potential (MEP)

Figure 6 shows two views of the MEP map of molecule 5 at 4.5 Å of the nuclei [60].

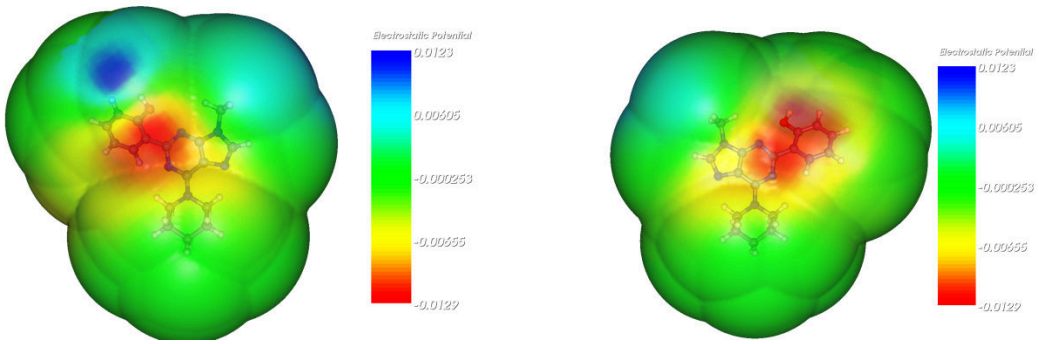

Figure 6: MEP map of molecule 4 at 4.5 Å of the nuclei

Figure 7 shows two views of the MEP map of molecule 12 at 4.5 Å of the nuclei.

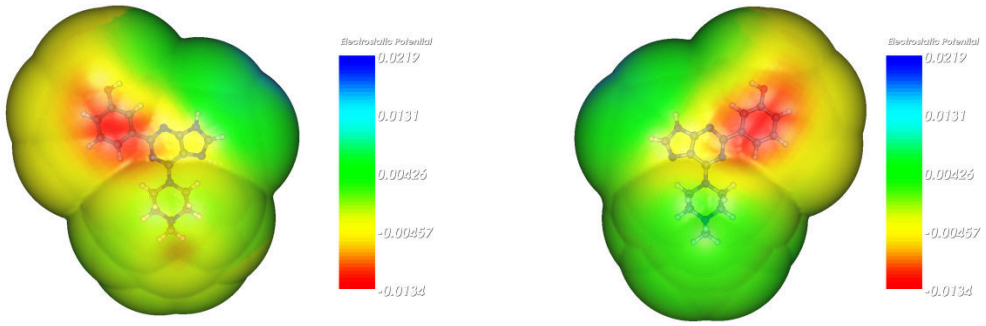

Figure 7: MEP map of molecule 12 at 4.5 Å of the nuclei

Figure 8 shows two views of the MEP map of molecule 16 at 4.5 Å of the nuclei.

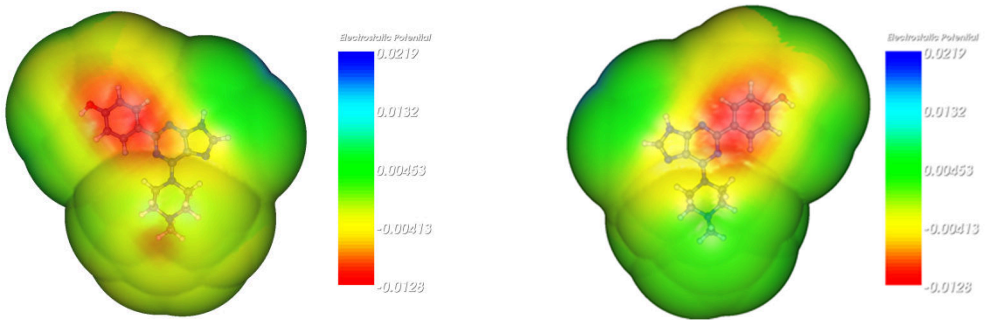

Figure 8: MEP map of molecule 16 at 4.5 Å of the nuclei

Figure 9 shows two views of the MEP map of molecule 20 at 4.5 Å of the nuclei.

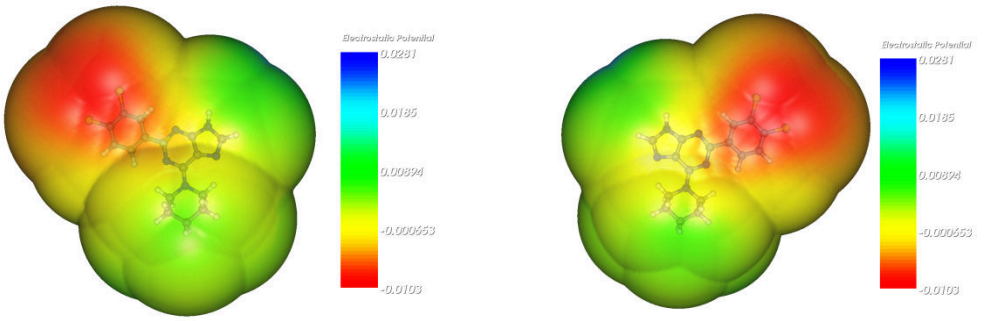

Figure 9: MEP map of molecule 20 at 4.5 Å of the nuclei

At about 4.5Å it is theoretically possible to identify some areas of the MEP associated with non-bond interactions such as π-cation or π-anion ones, helping to discard or not some suggestions resulting from the analysis of the statistical equations [61]. We do not know works following this line of thought but, to achieve this goal, MEP maps at 6, 5.5, 5 and 4.5Å seem necessary. A point to take into account is the conformation the molecule has at these distances (aqueous or hydrophobic environment?). Figures 10 to 13 show the MEP map surfaces with isovalues of ±0.0004 [62].

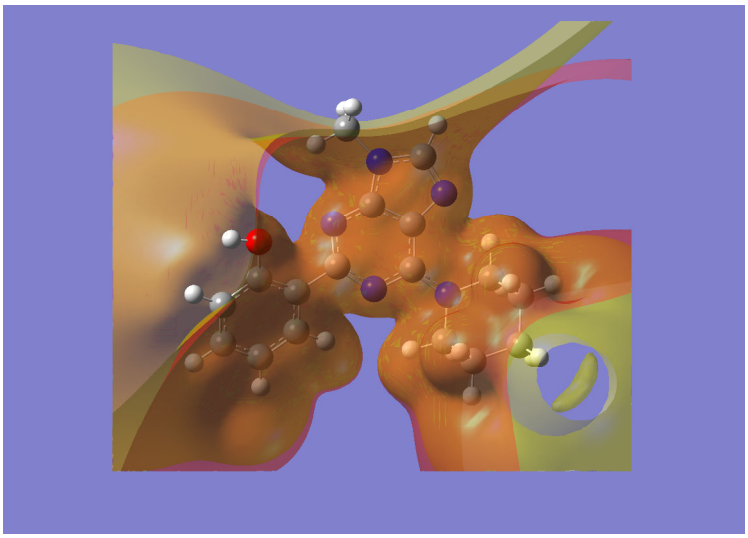

Figure 10: MEP map of molecule 5. The orange isovalue surface corresponds to negative values (-0.0004) and the yellow isovalue surface to positive values (0.0004)

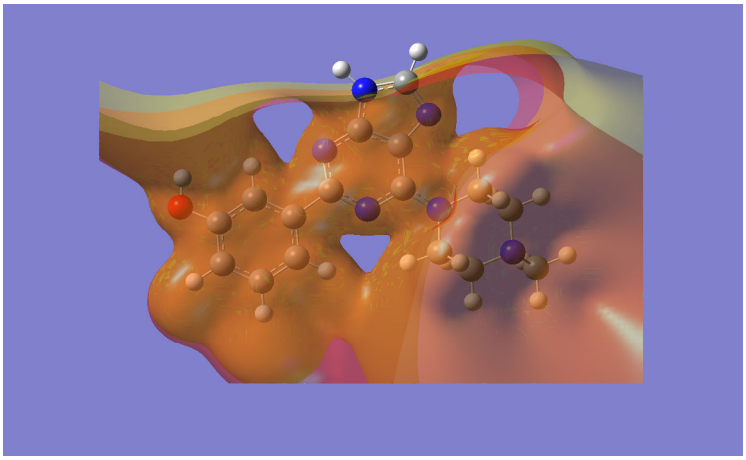

Figure 11: MEP map of molecule 12. The orange isovalue surface corresponds to negative values (-0.0004) and the yellow isovalue surface to positive values (0.0004)

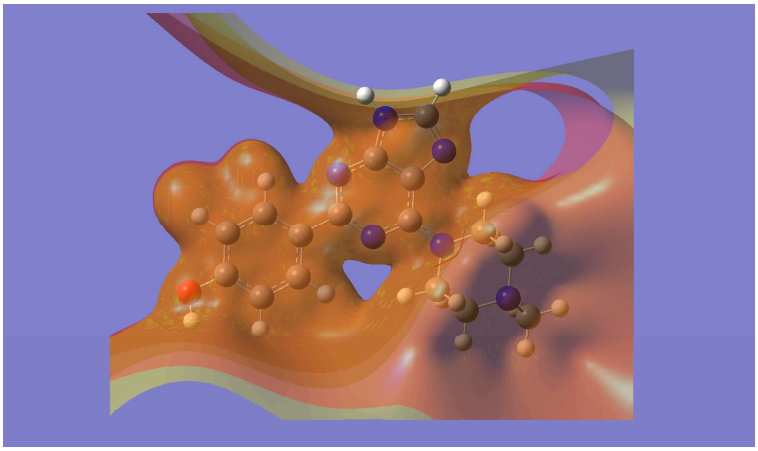

Figure 12: MEP map of molecule 16. The orange isovalue surface corresponds to negative values (-0.0004) and the yellow isovalue surface to positive values (0.0004)

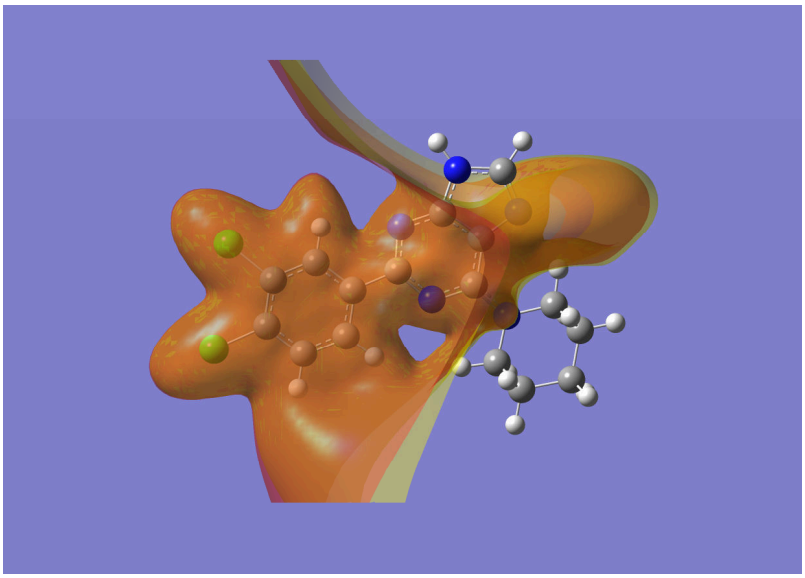

Figure 13: MEP map of molecule 20. The orange isovalue surface corresponds to negative values (-0.0004) and the yellow isovalue surface to positive values (0.0004)

At this short distance and for highly flexible molecules it is very difficult to find a relationship between, for example, MEP values at certain points and activity.

Discussion of the results for the percentage of inhibition of radioligand binding of test compounds at human adenosine receptors.

The biological activity analyzed above corresponds to the percentage of inhibition of radioligand binding of the tested compounds at a concentration of 10 μM. Therefore, what we want is to find the conditions to maximize this percentage.

Discussion of the results for the percentage of inhibition of radioligand binding of test compounds at human A_{2A} receptors [61, 63]**.**

Table 2 shows that the importance of variables in Eq. 2 is S_{12}^{E}(HOMO)*~ F_{20}(LUMO+1)*~ μ_{20}^{*}> F_{25}(HOMO)*>> F_{26}(HOMO)*~ F_{25}(HOMO-2)*> S_{15}^{N}(LUMO+2)*. The algebraic analysis of Eq. 2 shows that a large percentage of inhibition is associated with small numerical values for F_{26}(HOMO)*, large numerical values for S_{12}^{E}(HOMO)*, large (negative) numerical values for μ_{20}^{*}, large numerical values for F_{25}(HOMO)*, small numerical values for F_{20}(LUMO+1)*, large numerical values for F_{25}(HOMO-2)* and small numerical values for S_{15}^{N}(LUMO+2)*. Atom 26 is the substituent atom directly bonded to C-14 in ring D (H or Cl, see Table 1 and Fig. 2). Small numerical values for F_{26}(HOMO)* are associated with a large percentage of inhibition. Table 7 shows that $(HOMO)_{26}^{*}$ has sigma or pi nature. These small numerical values are obtained by substituting the molecules in such a way that the electron population of $(HOMO)_{26}^{*}$ be as small as possible. The other way is to substitute in such a way that the local $(HOMO)_{26}^{*}$ coincides this time with a molecule's molecular orbital that has more negative energy than the current one, enlarging the local atomic hardness of atom 26. In both cases the local molecular orbital becomes less reactive. On the other hand $(LUMO)_{26}^{*}$ does not coincide with the molecular LUMO but with high empty molecular orbitals. A possible explanation for both facts is that atom 26 should have a large local atomic hardness in such a way that it does not interact with the site. Atom 12 is a carbon atom in ring D (Fig. 2). Table 6 shows that $(HOMO)_{12}$* coincides with one of the three highest occupied Mos of the respective molecule and that $(LUMO)_{12}$* coincides with one of the two lowest empty Mos of the respective molecule. All local frontier Mos have a pi nature. Large negative numerical values for S_{12}^{E}(HOMO)* are associated with a large percentage of inhibition. The total atomic ESD of atom 12 is [43]:

$$S_{12}^{E*}=\sum_{m}\frac{F_{12,m}^{*}}{E_{m}^{*}}=\sum_{m}S_{12}^{E*}(m) \quad (4)$$

where the summation on m is over the occupied local molecular orbitals of atom 12. It is easy to see that the ESD value is always negative and that the dominant terms are the ones corresponding to the highest occupied local MOs. Therefore, large negative values will be obtained by shifting the MO energies toward zero, making $(HOMO)_{12}$* more reactive. This, in turn, suggests that atom 12 is interacting with an electron-deficient center. This interaction can be of pi-pi, pi-sigma and/or pi-cation kinds. Atom 20 is a sp^3carbon atom in ring A (Fig. 2). Table 7 shows that all local MOs have a sigma nature. Large (negative) numerical values for μ_{20}^{*} and small numerical values for F_{20}(LUMO+1)* are associated with a large percentage of inhibition. Regarding μ_{20}^{*}, this reactivity index is defined as [43, 44]:

$$\mu_{20}^{*}=\frac{E_{HOMO*,20}^{*}-E_{LUMO*,20}^{*}}{2} \quad (5)$$

where $E_{HOMO*,20}^{*}$ is the energy of $(HOMO)_{20}$* and $E_{LUMO*,20}^{*}$ is the energy of $(LUMO)_{20}$*. μ_{20}^{*} is a measure of the tendency of atom 20 to gain or lose electrons; a large negative value indicates a good electron acceptor while a small negative value implies a good electron donor. In this specific case the requirement imposed on this index indicates that atom 20 should be a good electron acceptor. But we must note that we have no indication about *how* to get these large negative values. One way is to make the Fukui index of the actual $(HOMO)_{20}$* zero, in such a way that an inner occupied MO of the molecule becomes the new $(HOMO)_{20}$*. This will make this occupied local frontier MO less reactive and μ_{20}^{*} more negative. The other way is by modifying the local MO localization in such a way that $(LUMO)_{20}$* coincides with the molecular LUMO. This produces a more reactive LUMO* and also a more negative μ_{20}*. Table 7 shows that this last method is the most suitable. The fact that small numerical values for F_{20}(LUMO+1)* are also required is not contradictory with the above facts if we think that perhaps there is a maximal amount of electronic charge that atom 20 could accept. Possible interactions can be π-σ, π-alkyl or alkyl-alkyl classes. Atom 15 is a carbon atom in ring D (Fig. 2). Small numerical values for S_{15}^{N}(LUMO+2)* are associated with a large percentage of inhibition. Table 6 shows that $(HOMO)_{15}$* corresponds with one of the three highest occupied MOs of the respective molecule and that $(LUMO)_{15}$* corresponds with one of the two lowest empty MOs of the corresponding molecule. All local frontier MOs have a pi nature in all cases. The nucleophilic superdelocalizability of the third lowest empty local molecular orbital of atom 15 is defined as [43]:

$$S_{15}^{N}(LUMO+2)*=\frac{F_{15}(LUMO+2)*}{E_{(LUMO+2)*}} \quad (6)$$

We can see from Eq. 6 that small numerical values for this reactivity index are generated by shifting upwards the MO energy (that is positive), making this MO less reactive. The other method is by modifying the local MO localization in such a way that $(LUMO+2)_{15}$* coincides with a still higher empty MO of the molecule. If we accept that the same condition applies to $(LUMO+1)_{15}$* and $(LUMO)_{15}$*, then we suggest that atom is interacting with an electron-deficient center. The interaction can be of π-π, π-σ and/or π-cation types. Atom 25 is the hydrogen atom directly bonded to C15 in ring D (see Table 1 and Fig. 2). Table 7 shows that all local MOs have a sigma nature. Large numerical values for F_{25}(HOMO)* and F_{25}(HOMO-2)* are associated with a large percentage of inhibition. This fact can be explained by suggesting that atom 25 is involved in a non-classical carbon hydrogen bond C15-H25….X (X=N, O). The simultaneous appearance of F_{25}(HOMO)* and F_{25}(HOMO-2)* with the same condition imposed on their numerical values gives some support to the idea that, when a term involving $(HOMO-2)_x$* appears in an equation in which similar terms associated with $(HOMO-1)_x$* and $(HOMO)_x$* do not appear, the conditions imposed on the numerical values of the term associated with $(HOMO-2)_x$* are also applied to the 'missing' similar terms associated with $(HOMO-1)_x$* and $(HOMO)_x$*. All the suggestions are displayed in the partial 2D pharmacophore of Fig. 14.

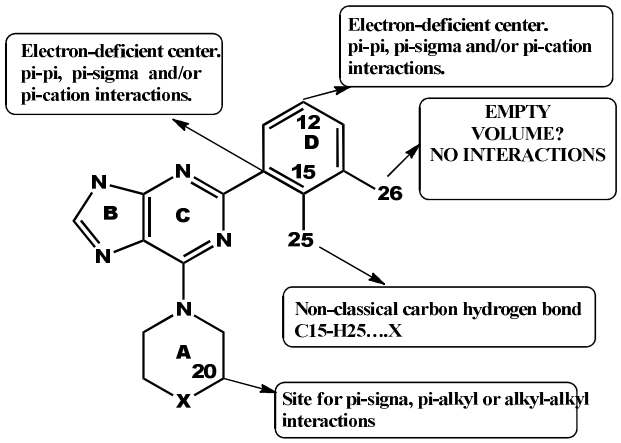

Figure 14: Partial 2D pharmacophore for the percentage of inhibition

Discussion of the results for the percentage of inhibition of radioligand binding of test compounds at human A_{2B} receptors.

Table 4 shows that the importance of variables in Eq. 3 is F_9(HOMO-2)*>> F_{24}(LUMO+1)*> S_{14}^E(HOMO-1)*> η_{18}^*. The algebraic analysis of Eq. 3 shows that a large percentage of inhibition is associated with small numerical values for F_9(HOMO-2)* and F_{24}(LUMO+1)*, large (negative) numerical values for S_{14}^E(HOMO-1)* and small numerical values for η_{18}^*. Atom 9 is a nitrogen atom in ring B (Fig. 2). A large percentage of inhibition is associated with small numerical values for F_9(HOMO-2)*. They are obtained by diminishing the electron population of $(HOMO-2)_9$*. Table 6 shows that $(HOMO-2)_9$* and $(HOMO-1)_9$* have a pi or sigma nature and that $(HOMO)_9$* has a pi nature. In all cases $(HOMO)_9$* coincides with the molecular HOMO and $(LUMO)_9$* coincides with one of the three highest occupied MOs of the respective molecule. $(LUMO)_9$* has a sigma nature in all cases. Considering that diminishing the electron population of the three highest occupied MOs diminishes their reactivity and capacity to interact with en electron-deficient center, we may suggest that atom 9 is interacting with an electron-rich center. The most probable interaction is a pi-anion one. Atom 24 is the substituent's atom directly bonded to C13 in ring D (Fig. 2, H, Cl or OH Table 1). A large percentage of inhibition is associated with small numerical values for F_{24}(LUMO+1)* making it less reactive. Therefore $(LUMO)_{24}$* will also become less reactive. In the case of the hydrogen substituents, both local frontier molecular orbitals are energetically far from the molecules frontier MOs (Table 7). In the case of chlorine substituents, Table 7 shows that $(LUMO+1)_{24}$* has a sigma or pi character, that $(LUMO+1)_{24}$* coincides with the molecular LUMO and that $(HOMO)_{24}$* coincides with the molecular HOMO. In the case of the oxygen atom (of the OH substituent), table 7 shows that the three highest occupied and the three lowest empty MOs coincide with the molecular equivalents. In the three cases, the requirement is the existence of empty MOs with a low or very low reactivity. We know that to diminish the numerical value of F_{24}(LUMO+1)* we need to diminish the electron population of this MO on atom 24. But there is a second way to get less reactive F_{24}(LUMO+1)* and F_{24}(LUMO)* MOs. It consists in eliminating the localization on atom 24 of these two MOs in such a way that, for example, the new $(LUMO)_{24}$* coincides now with a still higher empty MO of the molecule. These questions can be solved by electronic structure calculations of possible candidate structures before attempting a synthesis. Therefore, we suggest that inside the site there are residues able to accept a halogen interaction, a non-classical carbon hydrogen bond and possibly an O….H-X hydrogen bond. Atom 14 is a carbon atom in ring D (Fig. 2). Large (negative) numerical values for S_{14}^E(HOMO-1)* are associated with a high percentage of inhibition. Table 6 shows that $(HOMO)_{14}$* coincides with one of the two highest occupied molecular MOs and that $(HOMO-1)_{14}$* coincides with one of the five highest occupied molecular MOs. The necessary high negative numerical values are obtained by shifting upwards the $(HOMO-1)_{14}$* energy making it more reactive. The best situation is when $(HOMO-1)_{14}$* coincides with the second highest occupied MO of the molecule and $(HOMO)_{14}$* with the highest occupied MO of the molecule. This strongly suggests that atom 14 is interacting with an electron-deficient center through π-π,

π-σ and/or π-cation kinds. Atom 18 is a sp^3 carbon atom in ring A (Fig. 2). A large percentage of inhibition is associated with small numerical values for η_{18}^*. This reactivity index is simply the $(HOMO)_{18}$*-$(LUMO)_{18}$* energy gap. Theoretically, there is more than one way to reduce this gap. The first one is by shifting upwards the $(HOMO)_{18}$* energy. The second one is by shifting downwards the $(LUMO)_{18}$* energy. The third way is a combination of the first two. All local MOs have a sigma character. Table 6 shows that almost all $(HOMO)_{18}$* MOs coincide with the molecular HOMO of their corresponding molecule. The case of $(LUMO)_{18}$* is different because it corresponds to empty molecular MOs that are energetically very far from the molecular LUMO. Therefore, a first approach is to make coincide $(LUMO)_{18}$* with the corresponding frontier MO of the molecules. This will make the empty local MOs more reactive, suggesting that this atom interacts with an electron-rich center. The interactions could be π-alkyl, π-σ or alkyl ones. All the suggestions are displayed in the partial 2D pharmacophore of Fig. 15.

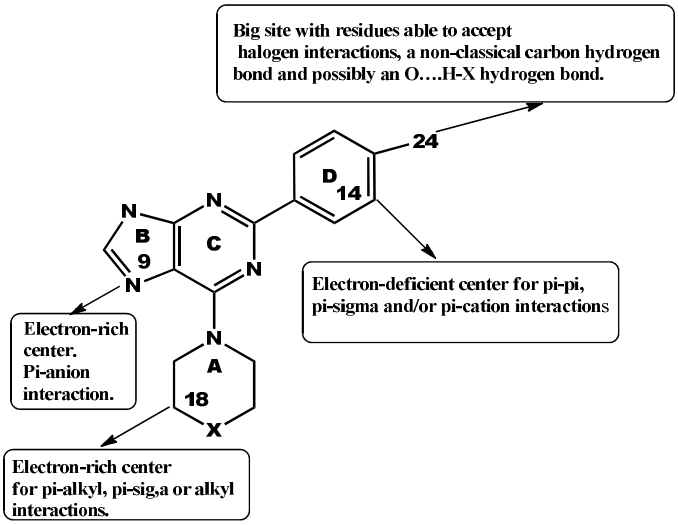

Figure 15: Partial 2D pharmacophore for the percentage of inhibition

Conclusion

In summary, we have searched for relationships between electronic structure and the percentage of inhibition of radioligand binding in human A2A and A2B adenosine receptors in a group of 2-aryladenine derivatives. We found statistically significant equations for both cases. Their analysis resulted in the suggestion of possible atom-site interactions that can be modified by appropriate substitutions to get more or less active compounds.

References

[1]. IJzerman, A. P.; Jacobson, K. A.; Müller, C. E.; Cronstein, B. N.; Cunha, R. A. International Union of Basic and Clinical Pharmacology. CXII: Adenosine Receptors: A Further Update. *Pharmacological Reviews* 2022, 74, 340-372.

[2]. Fredholm, B. B.; Frenguelli, B. G.; Hills, R.; IJzerman, A. P.; Jacobson, K. A.; Klotz, K.-N.; Linden, J.; Müller, C. E.; Schwabe, U.; Stiles, G. L. Adenosine receptors in GtoPdb v. 2021.2. *IUPHAR/BPS Guide to Pharmacology CITE* 2021, 2021.

[3]. López-Cruz, L.; Salamone, J. D.; Correa, M. Caffeine and selective adenosine receptor antagonists as new therapeutic tools for the motivational symptoms of depression. *Frontiers in Pharmacology* 2018, 9, 526.

[4]. Zhang, Y.; Wernly, B.; Cao, X.; Mustafa, S. J.; Tang, Y.; Zhou, Z. Adenosine and adenosine receptor-mediated action in coronary microcirculation. *Basic Research in Cardiology* 2021, 116, 1-17.

[5]. Spinozzi, E.; Baldassarri, C.; Acquaticci, L.; Del Bello, F.; Grifantini, M.; Cappellacci, L.; Riccardo, P. Adenosine receptors as promising targets for the management of ocular diseases. *Medicinal Chemistry Research* 2021, 30, 353-370.

[6]. Mazziotta, C.; Rotondo, J. C.; Lanzillotti, C.; Campione, G.; Martini, F.; Tognon, M. Cancer biology and molecular genetics of A3 adenosine receptor. *Oncogene* 2021, 1-8.

[7]. Atif, M.; Alsrhani, A.; Naz, F.; Imran, M.; Ullah, M. I.; Alameen, A. A.; Gondal, T. A.; Raza, Q. Targeting adenosine receptors in neurological diseases. *Cellular Reprogramming* 2021, 23, 57-72.

[8]. Effendi, W. I.; Nagano, T.; Kobayashi, K.; Nishimura, Y. Focusing on adenosine receptors as a potential targeted therapy in human diseases. *Cells* 2020, 9, 785.

[9]. van Calker, D.; Biber, K.; Domschke, K.; Serchov, T. The role of adenosine receptors in mood and anxiety disorders. *Journal of Neurochemistry* 2019, 151, 11-27.

[10]. Gorain, B.; Choudhury, H.; Yee, G. S.; Bhattamisra, S. K. Adenosine receptors as novel targets for the treatment of various cancers. *Current Pharmaceutical Design* 2019, 25, 2828-2841.

[11]. Choudhury, H.; Chellappan, D. K.; Sengupta, P.; Pandey, M.; Gorain, B. Adenosine receptors in modulation of central nervous system disorders. *Current Pharmaceutical Design* 2019, 25, 2808-2827.

[12]. Sek, K.; Mølck, C.; Stewart, G. D.; Kats, L.; Darcy, P. K.; Beavis, P. A. Targeting adenosine receptor signaling in cancer immunotherapy. *International Journal of Molecular Sciences* 2018, 19, 3837.

[13]. Jespers, W.; Schiedel, A. C.; Heitman, L. H.; Cooke, R. M.; Kleene, L.; van Westen, G. J.; Gloriam, D. E.; Müller, C. E.; Sotelo, E.; Gutiérrez-de-Terán, H. Structural mapping of adenosine receptor mutations: ligand binding and signaling mechanisms. *Trends in Pharmacological Sciences* 2018, 39, 75-89.

[14]. Borea, P. A.; Gessi, S.; Merighi, S.; Vincenzi, F.; Varani, K. Pharmacology of adenosine receptors: the state of the art. *Physiological Reviews* 2018, 98, 1591-1625.

[15]. Yu, F.; Zhu, C.; Ze, S.; Wang, H.; Yang, X.; Liu, M.; Xie, Q.; Lu, W.; Wang, Y. Design, Synthesis, and Bioevaluation of 2-Aminopteridin-7 (8 H)-one Derivatives as Novel Potent Adenosine A2A Receptor Antagonists for Cancer Immunotherapy. *Journal of Medicinal Chemistry* 2022.

[16]. Tosh, D. K.; Salmaso, V.; Campbell, R. G.; Rao, H.; Bitant, A.; Pottie, E.; Stove, C. P.; Liu, N.; Gavrilova, O.; Gao, Z.-G. A3 adenosine receptor agonists containing dopamine moieties for enhanced interspecies affinity. *European Journal of Medicinal Chemistry* 2022, 228, 113983.

[17]. Tosh, D. K.; Salmaso, V.; Rao, H.; Bitant, A.; Fisher, C. L.; Lieberman, D. I.; Vorbrüggen, H.; Reitman, M. L.; Gavrilova, O.; Gao, Z.-G. Truncated (N)-methanocarba nucleosides as partial agonists at mouse and human A3 adenosine receptors: Affinity enhancement by N 6-(2-phenylethyl) substitution. *Journal of Medicinal Chemistry* 2020, 63, 4334-4348.

[18]. Załuski, M.; Schabikowski, J.; Schlenk, M.; Olejarz-Maciej, A.; Kubas, B.; Karcz, T.; Kuder, K.; Latacz, G.; Zygmunt, M.; Synak, D. Novel multi-target directed ligands based on annelated xanthine scaffold with aromatic substituents acting on adenosine receptor and monoamine oxidase B. Synthesis, in vitro and in silico studies. *Bioorganic & Medicinal Chemistry* 2019, 27, 1195-1210.

[19]. Shaik, K.; Deb, P. K.; Mailavaram, R. P.; Chandrasekaran, B.; Kachler, S.; Klotz, K. N.; Jaber, A. M. Y. 7-Amino-2-aryl/hetero-aryl-5-oxo-5, 8-dihydro [1, 2, 4] triazolo [1, 5-a] pyridine-6-carbonitriles: Synthesis and adenosine receptor binding studies. *Chemical Biology & Drug Design* 2019, 94, 1568-1573.

[20]. Matos, M. J.; Vilar, S.; Vazquez-Rodriguez, S.; Kachler, S.; Klotz, K.-N.; Buccioni, M.; Delogu, G.; Santana, L.; Uriarte, E.; Borges, F. Structure-based optimization of coumarin hA3 adenosine receptor antagonists. *Journal of Medicinal Chemistry* 2019, 63, 2577-2587.

[21]. Deb, P. K.; Deka, S.; Borah, P.; Abed, S. N.; Klotz, K.-N. Medicinal chemistry and therapeutic potential of agonists, antagonists and allosteric modulators of A1 adenosine receptor: current status and perspectives. *Current Pharmaceutical Design* 2019, 25, 2697-2715.

[22]. Deb, P. K.; Chandrasekaran, B.; Mailavaram, R.; Tekade, R. K.; Jaber, A. M. Y. Molecular modeling approaches for the discovery of adenosine A2B receptor antagonists: current status and future perspectives. *Drug Discovery Today* 2019, 24, 1854-1864.

[23]. Dal Ben, D.; Lambertucci, C.; Buccioni, M.; Martí Navia, A.; Marucci, G.; Spinaci, A.; Volpini, R. Non-nucleoside agonists of the adenosine receptors: an overview. *Pharmaceuticals* 2019, 12, 150.

[24]. Chandrasekaran, B.; Samarneh, S.; Jaber, A. M.; Kassab, G.; Agrawal, N. Therapeutic potentials of A2B adenosine receptor ligands: current status and perspectives. *Current Pharmaceutical Design* 2019, 25, 2741-2771.

[25]. Areias, F.; Correia, C.; Rocha, A.; Brea, J.; Castro, M.; Loza, M. I.; Proença, M. F.; Carvalho, M. A. 2-Aryladenine derivatives as a potent scaffold for A1, A3 and dual A1/A3 adenosine receptor antagonists: Synthesis and structure-activity relationships. *Bioorganic & Medicinal Chemistry* 2019, 27, 3551-3558.

[26]. Varano, F.; Catarzi, D.; Falsini, M.; Vincenzi, F.; Pasquini, S.; Varani, K.; Colotta, V. Identification of novel thiazolo [5, 4-d] pyrimidine derivatives as human A1 and A2A adenosine receptor antagonists/inverse agonists. *Bioorganic & Medicinal Chemistry* 2018, 26, 3688-3695.

[27]. Shao, Y.M.; Ma, X.; Paira, P.; Tan, A.; Herr, D. R.; Lim, K. L.; Ng, C. H.; Venkatesan, G.; Klotz, K.N.; Federico, S. Discovery of indolylpiperazinylpyrimidines with dual-target profiles at adenosine A2A and dopamine D2 receptors for Parkinson's disease treatment. *PloS one* 2018, 13, e0188212.

[28]. Lambertucci, C.; Marucci, G.; Dal Ben, D.; Buccioni, M.; Spinaci, A.; Kachler, S.; Klotz, K.-N.; Volpini, R. New potent and selective A1 adenosine receptor antagonists as potential tools for the treatment of gastrointestinal diseases. *European Journal of Medicinal Chemistry* 2018, 151, 199-213.

[29]. Deb, P. K.; Mailavaram, R.; Chandrasekaran, B.; Kaki, V. R.; Kaur, R.; Kachler, S.; Klotz, K. N.; Akkinepally, R. R. Synthesis, adenosine receptor binding and molecular modelling studies of novel thieno [2, 3-d] pyrimidine derivatives. *Chemical Biology & Drug Design* 2018, 91, 962-969.

[30]. Chandrasekaran, B.; Deb, P. K.; Kachler, S.; Akkinepalli, R. R.; Mailavaram, R.; Klotz, K.-N. Synthesis and adenosine receptors binding studies of new fluorinated analogues of pyrido [2, 3-d] pyrimidines and quinazolines. *Medicinal Chemistry Research* 2018, 27, 756-767.

[31]. Gómez-Jeria, J. S.; Valenzuela-Hueichaqueo, N. J. The relationships between electronic structure and human A_1 adenosine receptor binding affinity in a series of triazolopyridine derivatives. *Chemistry Research Journal* 2020, 5, 226-236.

[32]. Gómez-Jeria, J. S.; Sánchez-Jara, B. An introductory theoretical investigation of the relationships between electronic structure and A1, A2A and A3 adenosine receptor affinities of a series of N6-8,9-trisubstituted purine derivatives. *Chemistry Research Journal* 2019, 4, 46-59.

[33]. The results presented here are obtained from what is now a routinary procedure. For this reason, all papers have a similar general structure. This model contains *standard* phrases for the presentation of the methods, calculations and results because they do not need to be rewritten repeatedly and because the number of possible variations to use is finite. See: Hall, S., Moskovitz, C., and Pemberton, M. 2021. Understanding Text Recycling: A Guide for Researchers. Text Recycling Research Project. Online at textrecycling.org.

[34]. Klopman, G.; Hudson, R. F. Polyelectronic perturbation treatment of chemical reactivity. *Theoretica chimica acta* 1967, 8, 165-174.

[35]. Klopman, G. Chemical reactivity and the concept of charge- and frontier-controlled reactions. *Journal of the American Chemical Society* 1968, 90, 223-234.

[36]. Peradejordi, F.; Martin, A. N.; Cammarata, A. Quantum chemical approach to structure-activity relationships of tetracycline antibiotics. *Journal of Pharmaceutical Sciences* 1971, 60, 576-582.

[37]. Gómez Jeria, J. S. La Pharmacologie Quantique. *Bollettino Chimico Farmaceutico* 1982, 121, 619-625.

[38]. Gómez-Jeria, J. S. On some problems in quantum pharmacology I. The partition functions. *International Journal of Quantum Chemistry* 1983, 23, 1969-1972.

[39]. Gómez-Jeria, J. S. Modeling the Drug-Receptor Interaction in Quantum Pharmacology. In *Molecules in Physics, Chemistry, and Biology*, Maruani, J., Ed. Springer Netherlands: 1989; Vol. 4, pp 215-231.

[40]. Gómez-Jeria, J. S.; Ojeda-Vergara, M. Parametrization of the orientational effects in the drug-receptor interaction. *Journal of the Chilean Chemical Society* 2003, 48, 119-124.

[41]. Barahona-Urbina, C.; Nuñez-Gonzalez, S.; Gómez-Jeria, J. S. Model-based quantum-chemical study of the uptake of some polychlorinated pollutant compounds by Zucchini subspecies. *Journal of the Chilean Chemical Society* 2012, 57, 1497-1503.

[42]. Alarcón, D. A.; Gatica-Díaz, F.; Gómez-Jeria, J. S. Modeling the relationships between molecular structure and inhibition of virus-induced cytopathic efects. Anti-HIV and anti-H1N1 (Influenza) activities as examples. *Journal of the Chilean Chemical Society* 2013, 58, 1651-1659.

[43]. Gómez-Jeria, J. S. *Elements of Molecular Electronic Pharmacology (in Spanish)*. 1st ed.; Ediciones Sokar: Santiago de Chile, 2013; p 104.

[44]. Gómez-Jeria, J. S. A New Set of Local Reactivity Indices within the Hartree-Fock-Roothaan and Density Functional Theory Frameworks. *Canadian Chemical Transactions* 2013, 1, 25-55.

[45]. Gómez-Jeria, J. S.; Soloaga Ardiles, C. E. A Density Functional Theory inquiry of the relationships between electronic structure and anticonvulsant activity in a series of 2,5-disubstituted thiadiazoles. *Chemistry Research Journal* 2022, 7, 55-68.

[46]. Gómez-Jeria, J. S.; Robles-Navarro, A.; Jaramillo-Hormazábal, I. A DFT analysis of the relationships between electronic structure and activity at D_2, 5-HT_{1A} and 5-HT_{2A} receptors in a series of Triazolopyridinone derivatives. *Chemistry Research Journal* 2022, 7, 6-28.

[47]. Gómez-Jeria, J. S.; Silva-Monroy, S. A quantum-chemical analysis of the relationships between electronic structure and inhibition of SARS-CoV-2 virus by a group of cyclic sulfonamide derivatives. *Chemistry Research Journal* 2021, 6, 54-70.

[48]. Gómez-Jeria, J. S.; Robles-Navarro, A.; Soza-Cornejo, C. A note on the relationships between electronic structure and serotonin 5-HT_{1A} receptor binding affinity in a series of 4-butyl-arylpiperazine-3-(1*H*-indol-3-yl)pyrrolidine-2,5-dione derivatives. *Chemistry Research Journal* 2021, 6, 76-88.

[49]. Gómez-Jeria, J. S.; Robles-Navarro, A.; Soto-Martínez, V. Quantum Chemical Analysis of the relationships between electronic structure and dopamine D_1 and D_5 receptor binding affinities in a series of 1-phenylbenzazepines. *Chemistry Research Journal* 2021, 6, 128-144.

[50]. Gómez-Jeria, J. S.; Ibertti-Arancibia, A. A DFT study of the relationships between electronic structure and dopamine D_1 and D_2 receptor affinity of a group of (S)-enantiomers of 11-(1,6-dimethyl-1,2,3,6-tetrahydropyridin-4-yl)-5*H*-dibenzo[b,e][1,4]diazepines. *Chemistry Research Journal* 2021, 6, 116-131.

[51]. Gómez-Jeria, J. S.; Crisóstomo-Cáceres, S. R.; Robles-Navarro, A. On the compatibility between formal QSAR results and docking results: the relationship between electronic structure and H5N1 (A/goose/Guangdong/SH7/2013) neuraminidase inhibition by some Tamiflu derivatives as an example. *Chemistry Research Journal* 2021, 6, 46-59.

[52]. Gómez-Jeria, J. S.; Soloaga Ardiles, C. E.; Kpotin, G. A. A DFT Analysis of the Relationships between Electronic Structure and Human κ, δ and μ Opioid Receptor Binding Affinity in a series of Diphenethylamines. *Chemistry Research Journal* 2020, 5, 32-46.

[53]. Gómez-Jeria, J. S.; Rojas-Candia, V. A DFT Investigation of the Relationships between Electronic Structure and D_2, 5-HT_{1A}, 5-HT_{2A}, 5-HT_6 and 5-HT_7 Receptor Affinities in a group of Fananserin derivatives. *Chemistry Research Journal* 2020, 5, 37-58.

[54]. Gómez-Jeria, J. S.; López-Aravena, R. A Theoretical Analysis of the Relationships between Electronic Structure and Dopamine D_4 Receptor Affinity in a series of compounds based on the classical D_4 agonist A-412997. *Chemistry Research Journal* 2020, 5, 1-9.

[55]. Gómez-Jeria, J. S.; González-Ponce, N. A Quantum-chemical study of the relationships between electronic structure and affinities for the serotonin transporter protein and the 5-HT_{1A} receptor in a series of 2H-pyrido[1,2-c]pyrimidine derivatives. *Chemistry Research Journal* 2020, 5, 16-31.

[56]. Frisch, M. J.; Trucks, G. W.; Schlegel, H. B.; Scuseria, G. E.; Robb, M. A.; Cheeseman, J. R.; Scalmani, G.; Barone, V.; Petersson, G. A.; Nakatsuji, H.; Li, X.; Caricato, M.; Marenich, A. V.; Bloino, J.; Janesko, B. G.; Gomperts, R.; Mennucci, B.; Hratchian, H. P. *Gaussian 16 16Rev. A.03*, Gaussian: Pittsburgh, PA, USA, 2016.

[57]. Gómez-Jeria, J. S. *D-Cent-QSAR: A program to generate Local Atomic Reactivity Indices from Gaussian16 log files*, v. 1.0; Santiago, Chile, 2020.

[58]. Gómez-Jeria, J. S. An empirical way to correct some drawbacks of Mulliken Population Analysis (Erratum in: J. Chil. Chem. Soc., 55, 4, IX, 2010). *Journal of the Chilean Chemical Society* 2009, 54, 482-485.
[59]. Statsoft. *Statistica v. 8.0*, 2300 East 14 th St. Tulsa, OK 74104, USA, 1984-2007.
[60]. Varetto, U. *Molekel 5.4.0.8*, Swiss National Supercomputing Centre: Lugano, Switzerland, 2008.
[61]. Gómez-Jeria, J. S.; Robles-Navarro, A.; Kpotin, G.; Garrido-Sáez, N.; Gatica-Díaz, N. Some remarks about the relationships between the common skeleton concept within the Klopman-Peradejordi-Gómez QSAR method and the weak molecule-site interactions. *Chemistry Research Journal* 2020, 5, 32-52.
[62]. Dennington, R. D.; Keith, T. A.; Millam, J. M. *GaussViev 5.0.8*, GaussViev 5.0.8, 340 Quinnipiac St., Bldg. 40, Wallingford, CT 06492, USA, 2000-2008.
[63]. Gómez-Jeria, J. S.; Kpotin, G. Some Remarks on The Interpretation of The Local Atomic Reactivity Indices Within the Klopman-Peradejordi-Gómez (KPG) Method. I. Theoretical Analysis. *Research Journal of Pharmaceutical, Biological and Chemical Sciences* 2018, 9, 550-561.